Monte Carlo Simulation and Measurement of Nanoscale n-MOSFETs

F. M. Bufler, Yoshinori Asahi, *Member, IEEE*, Hisao Yoshimura, *Member, IEEE*, Christoph Zechner, A. Schenk, and Wolfgang Fichtner, *Fellow, IEEE*

***Abstract*—The output characteristics of state-of-the-art n-MOSFETs with effective channel lengths of 40 and 60 nm have been measured and compared with full-band Monte Carlo simulations. The device structures are obtained by process simulation based on comprehensive secondary ion mass spectroscopy and capacitance–voltage measurements. Good agreement between the measured output characteristics and the full-band Monte Carlo simulations is found without any fitting of parameters and the on-currents are reproduced within 4%. The analysis of the velocity profiles along the channel confirms that the on-current is determined by the drift velocity in the source side of the channel. Analytic-band Monte Carlo simulations are found to involve an overestimation of the drain current in the nonlinear regime which becomes larger for increasing drain voltage and decreasing gate length. The discrepancy originates from a higher nonlinear drift velocity and a higher overshoot peak in bulk silicon which is due to differences in the band structures above 100 meV. The comparison between analytic-band and full-band Monte Carlo simulation therefore shows that the source-side velocity in the on-state is influenced by nonlinear and quasiballistic transport.**

***Index Terms*—Comparison measurement/simulation, Monte Carlo simulation, nanoscale MOSFETs, semiconductor device modeling.**

I. Introduction

As MOSFETs are scaled into the sub 0.1 μm regime, the on-current is increasingly determined by quasiballistic transport which is not adequately described by classical device simulation [1], [2]. An approach capable of taking ballistic transport effects into account is full-band Monte Carlo (FBMC) simulation [3], [4]. Therefore, many recent investigations have employed the Monte Carlo method to address the operation of nanoscale MOSFETs [2], [5]–[9] and advanced features such as elaborate models for impurity and surface roughness scattering have been studied [9]. However, since these works use the ensemble Monte Carlo approach, the high doping levels above 10^{20} cm^{-3} in state-of-the-art MOSFETs give rise to stability problems in the self-consistency scheme which can only be overcome by very short time steps on a subfemtosecond scale [10]. In order to reduce the computational effort, these Monte Carlo simulations were therefore restricted to simplified device structures with maximum doping levels considerably or even far below 1×10^{20} cm^{-3}. Consequently, none of the aforementioned works includes comparisons with experimental data, thus excluding the possibility to assess the relevance and validity of the models employed.

It is the aim of this work to bridge the gap between Monte Carlo device simulation and measurements by providing a comparison of the corresponding output characteristics of nanoscale MOSFETs. This will enable us to gauge the capability of Monte Carlo simulation to predict the scaling trend of the on-current in the sub-0.1-μm regime. To this end, we have performed calibrated process simulation of the measured MOSFET structures. On the other hand, we use the single-particle approach (SPARTA) to FBMC device simulation and achieve self-consistency by an iterative coupling scheme with the nonlinear Poisson equation [11]. Thereby the stability problem of the ensemble Monte Carlo approach is avoided and state-of-the-art MOSFETs can be simulated with affordable computational effort [12]. In addition, a comparison with other transport models (drift-diffusion, hydrodynamic and analytic-band Monte Carlo simulations) is used to clarify the origins which determine the on-current in nanoscale MOSFETs.

The paper is organized as follows. In Section II, we address the details of our Monte Carlo approach concerning band structure, scattering mechanisms, and numerical algorithms. We also present a comparison of the simulation results on the bulk level with experimental data in order to verify the models used. In Section III, details of the process simulation and calibration procedure are presented. Section IV contains the comparison of measured and simulated output characteristics for MOSFETs with different channel lengths as well as an interpretation of the results in terms of the velocity profiles along the channel. Finally, some conclusions are drawn in Section V.

II. Monte Carlo Model

In this section, the features of the simulation model are summarized. Most details concerning the band structure and the scattering processes as well as the propagation algorithm are given in [13] and [14]. Therefore, we report only the main aspects and concentrate on the modifications with respect to [13] and on the comparison with experimental bulk data.

The full-band structure is calculated by the nonlocal empirical pseudopotential approach including spin-orbit interaction and is stored on an equidistant mesh in momentum space with a spacing of $1/96 \times 2\pi/a$ with a denoting the lattice constant of

Manuscript received July 2, 2002; revised October 10, 2002. This work was supported in part by the Komission für Technologie und Innovation. The review of this paper was arranged by Editor R. Singh.

F. M. Bufler, A. Schenk, and W. Fichtner are with the Institut für Integrierte Systeme, ETH Zürich, CH-8092 Zürich, Switzerland (e-mail: bufler@iis.ee.ethz.ch).

Y. Asahi and H. Yoshimura are with Toshiba Corporation, Semiconductor Company, Isogo-ku 235-8522, Yokohama, Japan.

C. Zechner is with ISE Integrated Systems Engineering AG, CH-8008 Zürich, Switzerland.

Digital Object Identifier 10.1109/TED.2002.808420

0018-9383/03$17.00 © 2003 IEEE

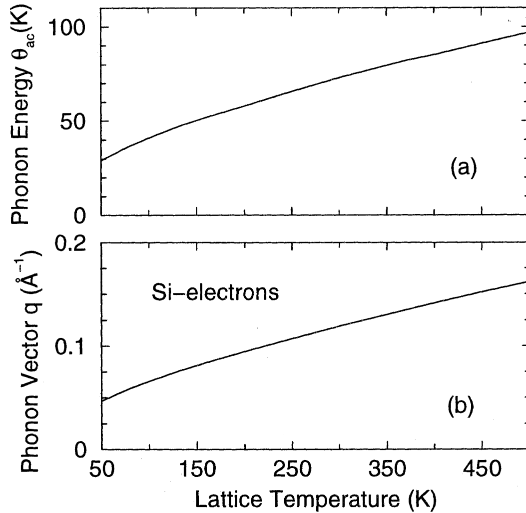

Fig. 1. Lattice temperature dependence of (a) the equivalent phonon temperature for acoustic intravalley scattering defined via $\theta_{\rm ac} = \langle \hbar\omega(q) \rangle / k_B$ and (b) of the corresponding mean modulus of the phonon wave vector given by $\sqrt{\langle q^2 \rangle}$.

silicon. The scattering mechanisms comprise phonon scattering, impact ionization, impurity scattering, and surface roughness scattering [13]. The phonon scattering model includes three f-type and three g-type intervalley scattering processes using exactly the same coupling constants as Jacoboni and Reggiani [15] and acoustic intravalley scattering. Intravalley scattering is treated inelastically with a constant phonon energy which is obtained by an averaging procedure from the acoustic phonon dispersion in analogy to a corresponding approach in the case of holes [16]. Using the parametrization of the phonon dispersion given in [17], as a first step the modulus of the phonon wave vector, $q = ||\mathbf{k}' - \mathbf{k}||$, is averaged over a sphere in the spirit of an isotropic, parabolic band structure ($\mathbf{k}'$ and $\mathbf{k}$ are the electron's momentum after and before the scattering event, respectively). The result is $q = (4/3)k$. Then the phonon energy is averaged according to

$$k_B \theta_{\rm ac} \equiv \hbar\omega_{ac} = \frac{\int d\epsilon \hbar\omega \left(\frac{4}{3}k(\epsilon)\right) \mathcal{D}(\epsilon) e^{-\epsilon/(k_b T)}}{\int d\epsilon \mathcal{D}(\epsilon) e^{-\epsilon/(k_b T)}} \quad (1)$$

where $\mathcal{D}(\epsilon)$ denotes the density of states, k_B is the Boltzmann constant, and $k(\epsilon) = \sqrt{2m(\epsilon)\epsilon}/\hbar$ with the effective mass $m(\epsilon)$ taken to be the energy-dependent effective density-of-states mass. The same procedure is applied to the square of the phonon wave vector appearing in the expression for the transition probability [16], [17]. As a result, the acoustic phonon energy and the phonon vector depend on the lattice temperature as shown in Fig. 1. Adjusting the acoustic intravalley deformation potential $\mathcal{E}$ appearing in the scattering rate (see [16] for the formula) yields with this model $\mathcal{E} = 7.73$ eV. It is true that this approximation becomes inaccurate for high fields, but this does not impair the accuracy of the simulation because in the high-field regime intervalley processes are dominant. The model ensures that energy dissipation occurs at all fields and lattice temperatures since the acoustic phonon energy is always smaller than the thermal energy. Nevertheless, it turns

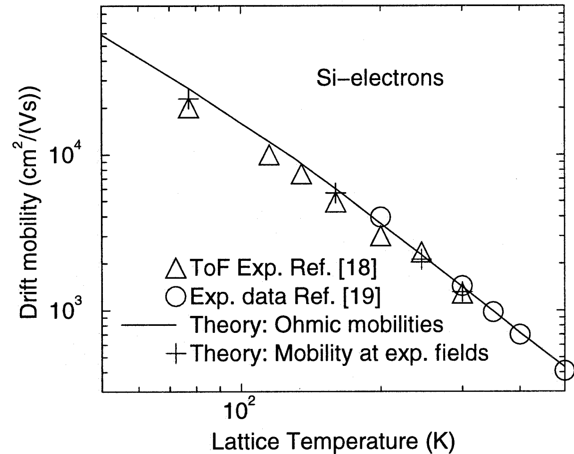

Fig. 2. Theoretical and experimental results for the drift mobility as a function of the lattice temperature.

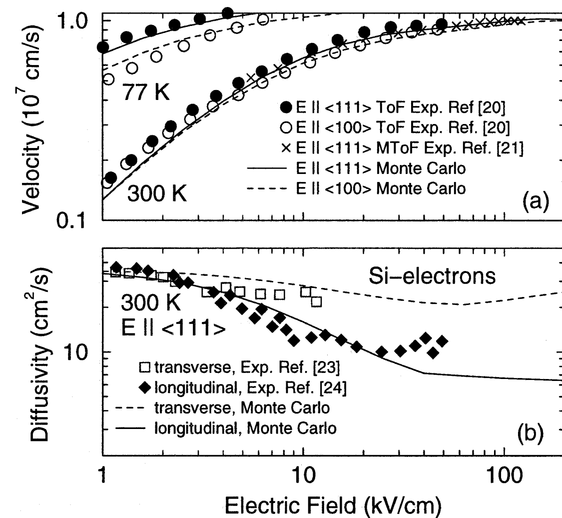

Fig. 3. Comparison between theoretical and experimental results for (a) the velocity-field characteristics in the crystallographic $\langle 111 \rangle$ and $\langle 100 \rangle$ directions at lattice temperatures of 77 and 300 K and for (b) the field-dependence of the transverse and longitudinal diffusion constant in $\langle 111 \rangle$ direction at 300 K.

out that the effect of intravalley scattering by inelastic acoustic phonons is mostly negligible in contrast to the case of holes where the high-energy tail of the energy distribution is significantly enhanced in comparison with the elastic equipartition approximation [16].

However, with this model we find in agreement with [17], where the full acoustic phonon dispersion was taken into account, that the fields applied in time-of-flight measurements of the low-field mobility [18] were somewhat too large at low lattice temperatures to be in the ohmic regime. Monte Carlo simulations performed at the fields applied in the experiments therefore improve the agreement between theory and measurements at low lattice temperatures, as can be seen in Fig. 2, where further experimental data are also shown [19]. A comparison of the results of the Monte Carlo model with experiments in the high-field regime is shown in Fig. 3. In Fig. 3(a), the simulated velocity-field characteristics in the crystallographic $\langle 100 \rangle$ and

$\langle 111 \rangle$ directions at 77 and 300 K are displayed together with corresponding time-of-flight (ToF) measurements [20], [21]. Another measurable quantity, which can serve as an independent possibility to verify the Monte Carlo model, is the diffusivity tensor D_{ij} where i and j stand for the Cartesian coordinates. It can be computed from the velocity autocorrelation function under steady-state conditions according to [22]

$$D_{ij} = \int_0^\infty dt \langle \delta v_i(0) \delta v_j(t) \rangle \quad (2)$$

where the brackets refer to ensemble average. Projection in the direction parallel and perpendicular to the electric field leads to the longitudinal and transverse diffusion coefficients, respectively, which can be seen in Fig. 3(b) in comparison to experimental data [23], [24]. In conclusion, a good overall agreement has been found between the present Monte Carlo model and experimental bulk data under various conditions as depicted in Figs. 2 and 3.

Another difference with respect to [13] concerns the realization of the ohmic boundary condition where the single electron is now injected directly at the contact from a velocity-weighted Maxwellian.

Finally, self-consistency of the Monte Carlo device simulation is achieved by an iteration of the frozen-field simulations of [13] with solutions of the nonlinear Poisson equation as proposed by Venturi *et al.* [11]. The validity and efficiency of this scheme have been demonstrated in [12].

III. Process Simulation and Calibration

The lightly doped drain (LDD) n-MOSFETs feature a physical oxide thickness of $t_{OX} = 2$ nm, a retrograde channel doping, and maximum doping levels of around 5×10^{20} cm^{-3}. The junction depth between the source/drain (S/D) and the well regions was 140 nm. The junction depth between the halo doping and the S/D extension was around 20 nm, allowing transistor operation for devices with gate lengths down to about 60–80 nm. The device structures were obtained by calibrated process simulation [25]. This calibration was based on: 1) comprehensive secondary ion mass spectroscopy (SIMS) data of profiles corresponding to the fabrication process; 2) capacitance–voltage (C–V) measurements; and 3) electrical data of n-MOSFETs of various gate lengths for 48 experimental splits including different implantation and annealing conditions. The process simulation included the pair diffusion framework, Monte Carlo simulation of ion implantation, interstitial and dopant clustering models, and dose loss modeling. The calibration led to a good agreement between SIMS profiles and 1D process simulation results and between measured and simulated C–V and threshold voltage (VT) roll-off curves. An analysis of measured and simulated VT curves allows an evaluation of the accuracy achieved. In a comparison made for 13 split variants with varying parameters for channel, extension and halo implantation, and annealing, the mismatch between measured and simulated threshold voltages of the n-MOSFETs was on average less than 25 mV for gate lengths between 80 nm and 10 μm. The predictive capability of the

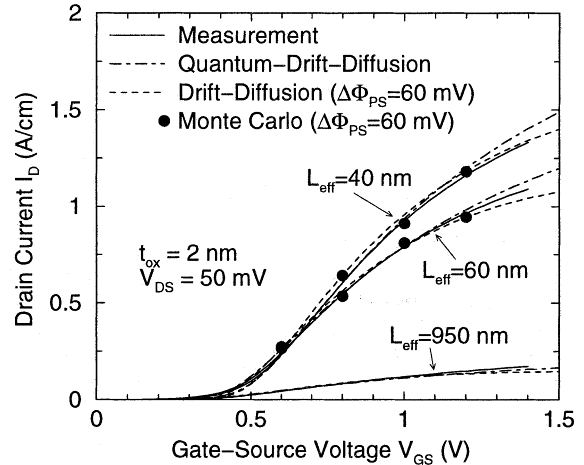

Fig. 4. Transfer characteristics of three n-MOSFETs with effective channel lengths of 40, 60, and 950 nm. The measurements are compared to simulations with the QDD, the classical drift-diffusion (DD) and the FBMC model (in the DD and the FBMC model, the threshold voltage shift due to quantization is taken into account by a work function difference $\Delta\Phi_{PS}$ between polysilicon and undoped silicon of 60 mV).

calibrated models is thus in the range of ± 25 mV for moderate variations of the fabrication process. In this calibration, the device simulation results were obtained with DESSIS [26] using a quantum drift-diffusion (QDD) model (also referred to as density gradient model) [27], bandgap narrowing according to Slotboom [28] equally attributed to valence and conduction band-edge, and surface mobility degradation as proposed by Darwish *et al.* [29]. Note that the band-gap narrowing model and the assignment to conduction and valence band-edge are still affected by uncertainties and should be investigated in more detail in the future.

Starting from these structures, fine-tuning was performed on the classical device simulation level to enable a comparison with Monte Carlo device simulation. The parameters of the surface mobility model were tuned such that the measured drain currents at a drain voltage of $V_{DS} = 50$ mV are reproduced for all gate lengths, i.e., for $L_G = 980$, 90, and 65 nm (corresponding to effective gate lengths of $L_{\rm eff} = 950$, 60, and 40 nm). While the default parameters of the Darwish model [29] are able to reproduce the long-channel device characteristics, agreement for all gate lengths with one parameter set required a strong modification of the parameters C and λ in this model. Then the quantum mechanical threshold voltage shift is taken into account via a work function difference between polysilicon and undoped silicon of $\Delta\Phi_{PS} = 60$ mV, both for the classical drift-diffusion and the Monte Carlo model. This simplification with respect to the density gradient model was necessary, because the present Monte Carlo model does not include the quantum effect explicitly. The result of this procedure is shown in Fig. 4. In contrast to the drift-diffusion model, however, no adjustment of the specular/diffusive surface scattering model was necessary in the case of Monte Carlo. The default value of 15% for the percentage of diffusive scattering determined in [30] already reproduces the measured drain currents both for $L_{\rm eff} = 60$ nm and $L_{\rm eff} = 40$ nm at $V_{DS} = 50$ mV as can be seen in Fig. 4.

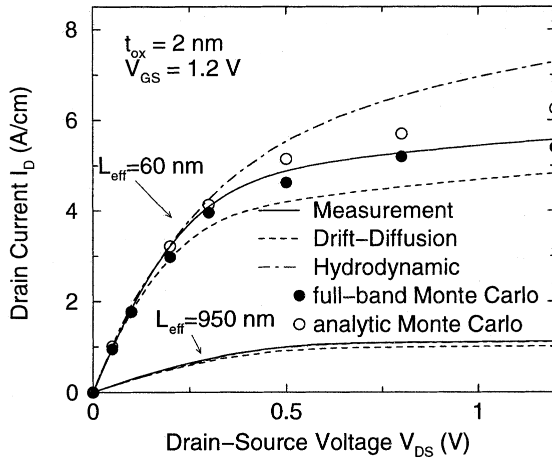

Fig. 5. Measured output characteristics of two n-MOSFETs with effective lengths of 60 and 950 nm in comparison with simulations based on the DD model, the hydrodynamic model, the Monte Carlo model with an analytic-band description, and the FBMC model.

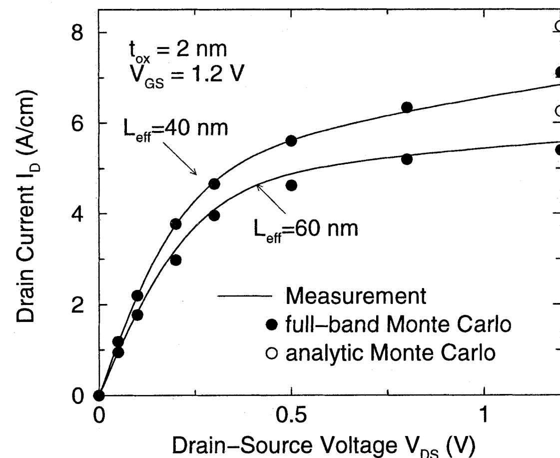

Fig. 6. Measured output characteristics of two n-MOSFETs with effective lengths of 40 and 60 nm in comparison with FBMC simulations. The on-currents resulting from the Monte Carlo model based on an analytic-band description are also shown.

IV. Simulation Results and Discussion

In this section, the output characteristics for the n-MOSFETs are simulated at a gate voltage of $V_{GS} = 1.2$ V using the models described before without any changes. In addition, the FBMC simulations are also compared to analytic-band Monte Carlo (ABMC) simulations. The analytic-band structure consists of one anisotropic and nonparabolic conduction band as, e.g., employed by Jacoboni and Reggiani [15] and is stored in a discretized form in a table in analogy to the full-band model. The quantum mechanical threshold voltage shift is always taken into account via $\Delta\Phi_{PS} = 60$ mV.

The results of different simulation approaches in comparison with the measurements are displayed in Fig. 5 for the transistors with an effective gate length of $L_{\text{eff}} = 950$ nm and $L_{\text{eff}} = 60$ nm, respectively. It turns out that the standard hydrodynamic model (with a constant energy relaxation time of $\tau_w = 0.3$ ps) systematically improves upon the drift-diffusion model in the linear regime, i.e., up to $V_{DS} = 0.3$ V for $L_{\text{eff}} = 60$ nm and for the whole output characteristics in the case of $L_{\text{eff}} = 950$ nm. However, in the short-channel device the deviation for the on-current (the drain current I_D at $V_{DS} = V_{GS} = 1.2$ V) is much stronger in the hydrodynamic case than for the DD model. The hydrodynamic (HD) simulation overestimates the on-current by 30% versus an underestimation of 14% by the drift-diffusion approach, whereas the FBMC simulation reproduces the on-current within 3%.

Of course, the agreement of the computationally efficient classical simulators (CPU time for the on-current in the order of one day for Monte Carlo, 1 h for HD and 10 min for DD) with the measurements can be improved by adjusting, e.g., the parameters in the Caughey–Thomas model for the velocity-field characteristics as proposed in [2]. For example, the measured on-current of the n-MOSFET with $L_{\text{eff}} = 60$ nm could be reproduced by the DD model when using a saturation velocity of $v_{\text{sat}} = 1.35 \times 10^7$ cm/s and $\beta \approx 1.13$ in the Caughey–Thomas model. However, with these parameters, the on-current was only slightly increased for the long-channel device, while it was already overestimated by more than 5% in the n-MOSFET with $L_{\text{eff}} = 40$ nm. Besides being in contradiction to the established experimental bulk velocity-field characteristics, the two parameters will also depend on the technology as is suggested by the difference of our values to those extracted in [2].

Furthermore, it can be seen in Fig. 5 that the results of the ABMC simulations agree with the FBMC results as expected for low drain voltages, but overestimate the drain current for increasing drain voltages (the overestimation of the on-current is even stronger for smaller gate lengths as depicted in Fig. 6). These deviations can be traced back to the different band structures. Above 100 meV, the analytic band structure leads to an underestimation of the density of states and an overestimation of the group velocity (averaged over an equienergy surface) as is shown in [31, Figs. 2 and 3]. This is the reason why the analytic-band Monte Carlo simulation significantly overestimates the bulk drift-velocity at medium field strengths, as can be seen in [32, Fig. 2] (note that there is a difference at higher energies between a true analytic-band structure and a discretized version in the Brillouin zone because in the true analytic case there are also allowed states outside the Brillouin zone; we have checked that the resulting differences are neglible for the drift velocity). In addition, we have also computed the transient bulk velocity overshoot after a sudden application of a 100-kV/cm field and the mean thermal injection velocity. It turns out that the Monte Carlo simulation based on the analytic-band model overestimates the overshoot peak, which is caused by quasi-ballistic transport, by 21%, whereas the injection velocity is only 2% too high. Since the thermal injection velocity as well as the low-field mobility are the same in both band models, it can be concluded that the overestimation of the drain current at higher drain voltages is due to an overestimation of nonlinear and quasiballistic transport by the analytic band structure.

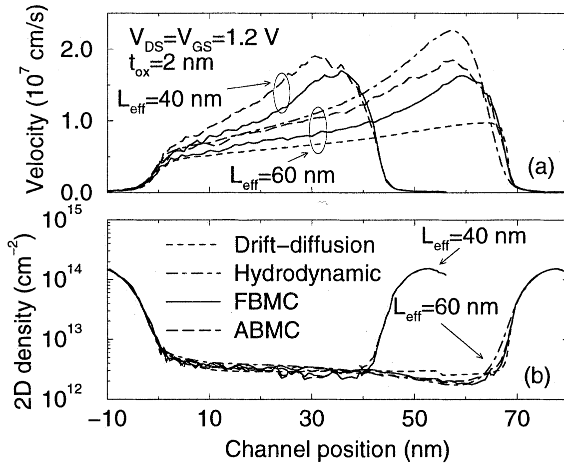

Fig. 7. Profiles of (a) the drift velocity and (b) the 2-D inversion electron density along the channel resulting from the ABMC and FBMC models for the 40-nm n-MOSFET and according to the DD, HD, ABMC and FBMC models for the 60-nm n-MOSFET. The position where the longitudinal field changes the sign at the source side of the channel is taken as zero.

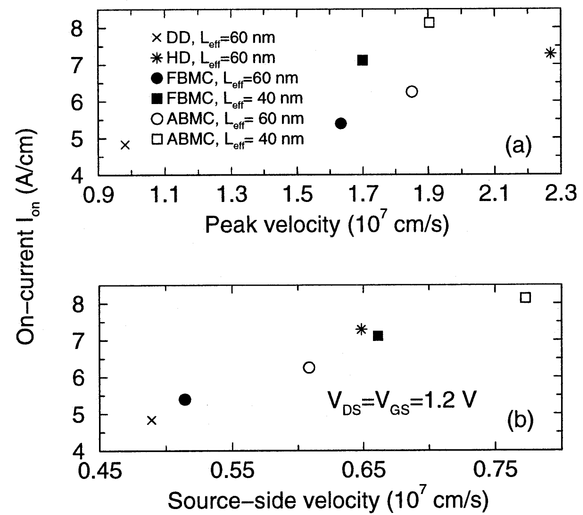

Fig. 8. On-currents according to the different transport models (DD, HD, ABMC, and FBMC) and gate lengths ($L_{\mathrm{eff}} = 40$ nm and $L_{\mathrm{eff}} = 60$ nm) as a function of (a) the peak velocity of the respective transport model at the drain side of the channel and (b) the corresponding source-side velocity (at 6 nm from the position where the longitudinal field changes the sign at the source side of the channel).

The scaling trend of the on-current is addressed in Fig. 6 where FBMC simulations and measurements of the output characteristics are compared in nanoscale MOSFETs with effective gate lengths of $L_{\mathrm{eff}} = 60$ nm and $L_{\mathrm{eff}} = 40$ nm. Good agreement between measurement and FBMC simulation can be seen. The on-current is increased by 23% by reducing the gate length L_G from 90 to 65 nm, and for both gate lengths the on-current is reproduced within 4% by the FBMC simulation.

The different values for the on-current occurring at different gate lengths or resulting from different simulation models can be explained in terms of the profiles of internal quantities along the channel (compare, e.g., [2] and [12]). The drift velocity along the channel, averaged with the electron density perpendicularly to the Si/SiO_2 interface, and the two-dimensional (2-D) inversion electron density, obtained by integrating the electron density perpendicularly to the interface, are shown in Fig. 7 for different gate lengths and simulation models. The origin of the lateral position is taken for both gate lengths as the position where the longitudinal field changes its sign at the source side of the channel. It can be seen that the variations between the different configurations at the source-side of the channel are stronger for the drift velocity than for the inversion density which is essentially only determined by the solution of the Poisson equation. Since charge conservation implies that the current remains constant inside the channel, the origin for the different results of the transport models for the on-current must mainly lie in the different source-side velocities, as was already pointed out previously by Lundstrom and collaborators [1], [33]–[36]. In the following, we examine this conclusion in more detail. At first we compare different simulation models for the MOSFET with $L_{\mathrm{eff}} = 60$ nm. It can be seen that the velocity in the source side of the channel is larger for the FBMC model than in the case of the DD simulation and is even much more enhanced in the hydrodynamic model. This correlates with the order and magnitude of the on-currents in Fig. 5. Comparing these velocity profiles with the FBMC result for the MOSFET with $L_{\mathrm{eff}} = 40$ nm, it becomes clear that the on-current is determined by the source-side velocity and not by the velocity overshoot peak at the drain side of the channel. The on-current of the FBMC model in the 40-nm MOSFET almost coincides with the on-current of the hydrodynamic model in the 60-nm MOSFET despite a much stronger velocity overshoot peak of the hydrodynamic model. It is indeed the magnitude of the velocities in the source side of the channel which is equal in both cases and hence leads to a similar on-current. This interpretation is also supported by the fact that the FBMC simulation leads to almost no increase of the overshoot peak in the smaller transistor, but involves nevertheless a much higher on-current which is again in agreement with the higher source-side velocity. Similarly, the higher on-currents of the ABMC model as compared to the FBMC model correspond also to higher source-side velocities. The above observations are summarized quantitatively in Fig. 8 where the on-current is plotted as a function of (a) the peak velocities in the drain-side of the channel and (b) the velocities near the source-side of the channel in the different configurations. It can be seen that there is no clear relation between the on-current and the peak velocities. In contrast, the on-current depends almost linearly on the source-side velocities. This supports the conclusion that the source-side velocity is decisive for the on-current whereas the velocity overshoot peak in the drain-side of the channel is of minor importance.

Having established the crucial role of the source-side velocity for the on-current, we finally turn to the microscopic mechanisms which determine the source-side velocity itself within the framework of the semiclassical Boltzmann transport equation. The electrons experience strong impurity scattering in the highly-doped source region and are therefore near equilibrium with a velocity corresponding to the low-field mobility as they approach the channel. In the channel, they are after a very short distance exposed to a high electric field. This situation is there-

fore similar to that of an ensemble of bulk electrons in equilibrium when suddenly a constant field is applied. Depending on the field strength the electrons will adopt on a certain distance in the channel (equivalent to a time interval in bulk silicon) a velocity corresponding to the nonlinear velocity-field characteristics or, for a stronger field, a velocity which is larger than would correspond to the local field strength (not necessarily larger than the saturation velocity). The comparison between the ABMC and the FBMC simulation does indeed support the above interpretation. The low-field mobility is the same for both band models and consequently the drain current in the linear regime of the output characteristics in Fig. 5 is the same. As the drain voltage becomes higher (or the gate length decreases as in Fig. 6), the overestimation of the drain current by the analytic-band model increases in agreement with an overestimation of the nonlinear bulk velocity and the bulk overshoot peak. Since both the low-field mobilities and the mean thermal injection velocities, with which electrons are injected, e.g., from an ideal ohmic contact by virtue of a tunneling process, are nearly the same in both band models, the strong difference in the on-currents between the ABMC and the FBMC model might point to a certain limitation of nanoscale MOSFET models relying only on injection velocity and backscattering.

V. Conclusion

FBMC simulations and measurements of the output characteristics of nanoscale n-MOSFETS have been compared. Good agreement is observed without any parameter fitting of the FBMC model. A comparison of the FBMC simulations with DD, HD, and ABMC simulation shows that the on-current is related to the velocity in the source side of the channel which is itself determined by nonlinear and quasi-ballistic transport. The good agreement with the measurements demonstrates that FBMC simulation can be regarded as a reliable tool for estimating the on-currents of nanoscale MOSFETs.

References

[1] K. Banoo and M. S. Lundstrom, “Electron transport in a model Si transistor,” *Solid-State Electron.*, vol. 44, pp. 1689–1695, 2000.

[2] J. D. Bude, “MOSFET modeling into the ballistic regime,” in *Proc. SISPAD*, Seattle, WA, Sept. 2000, pp. 23–26.

[3] M. V. Fischetti and S. E. Laux, “Monte Carlo analysis of electron transport in small semiconductor devices including band-structure and space-charge effects,” *Phys. Rev. B*, vol. 38, pp. 9721–9745, 1988.

[4] K. Hess, Ed., *Monte Carlo Device Simulation: Full Band and Beyond*. Boston, MA: Kluwer, 1991.

[5] A. Duncan, U. Ravaioli, and J. Jakumeit, “Full-band Monte Carlo investigation of hot carrier trends in the scaling of metal–oxide-semiconductor field-effect transistors,” *IEEE Trans. Electron Devices*, vol. 45, pp. 867–876, 1998.

[6] C. Jungemann, S. Keith, M. Bartels, and B. Meinerzhagen, “Efficient full-band Monte Carlo simulation of silicon devices,” *IEICE Trans. Electron.*, vol. E82-C, pp. 870–879, 1999.

[7] C. Jungemann and B. Meinerzhagen, “Impact of the velocity overshoot on the performance of NMOSFET’s with gate lengths from 80 nm to 250 nm,” in *Proc. ESSDERC*, vol. 29, H. E. Maes, R. P. Mertens, G. Declerck, and H. Grünbacher, Eds., Leuven, Belgium, 1999, pp. 236–239, Editions Frontières.

[8] W. J. Gross, D. Vasileska, and D. K. Ferry, “Ultrasmall MOSFETs: The importance of the full Coulomb interaction on device characteristics,” *IEEE Trans. Electron Devices*, vol. 47, pp. 1831–1837, 2000.

[9] G. F. Formicone, M. Saraniti, D. Z. Vasileska, and D. K. Ferry, “Study of a 50-nm nMOSFET by ensemble Monte Carlo simulation including a new approach to surface roughness and impurity scattering in the Si inversion layer,” *IEEE Trans. Electron Devices*, vol. 49, pp. 125–132, 2002.

[10] P. W. Rambo and J. Denavit, “Time stability of Monte Carlo device simulation,” *IEEE Trans. Computer-Aided Design*, vol. 12, pp. 1734–1741, 1993.

[11] F. Venturi, R. K. Smith, E. C. Sangiorgi, M. R. Pinto, and B. Riccó, “A general purpose device simulator coupling Poisson and Monte Carlo transport with applications to deep submicron MOSFET’s,” *IEEE Trans. Computer-Aided Design*, vol. 8, pp. 360–369, 1989.

[12] F. M. Bufler, C. Zechner, A. Schenk, and W. Fichtner, “Self-consistent single-particle simulation,” in *Proc. SISPAD*, Kobe, Japan, Sept. 2002, pp. 159–162.

[13] F. M. Bufler, A. Schenk, and W. Fichtner, “Efficient Monte Carlo device modeling,” *IEEE Trans. Electron Devices*, vol. 47, pp. 1891–1897, 2000.

[14] ——, “Proof of a simple time-step propagation scheme for Monte Carlo simulation,” *Math Comput. Simulation*, vol. 62, pp. 323–326, 2003.

[15] C. Jacoboni and L. Reggiani, “The Monte Carlo method for the solution of charge transport in semiconductors with application to covalent materials,” *Rev. Mod. Phys.*, vol. 55, pp. 645–705, 1983.

[16] F. M. Bufler, A. Schenk, and W. Fichtner, “Simplified model for inelastic acoustic phonon scattering of holes in Si and Ge,” *J. Appl. Phys.*, vol. 90, pp. 2626–2628, 2001.

[17] B. Fischer and K. R. Hofmann, “A full-band Monte Carlo model for the temperature dependence of electron and hole transport in silicon,” *Appl. Phys. Lett.*, vol. 76, pp. 583–585, 2000.

[18] C. Canali, C. Jacoboni, F. Nava, G. Ottaviani, and A. Alberigi-Quaranta, “Electron drift velocity in silicon,” *Phys. Rev. B*, vol. 12, pp. 2265–2284, 1975.

[19] M. A. Green, “Intrinsic concentration, effective densities of states, and effective mass in silicon,” *J. Appl. Phys.*, vol. 67, pp. 2944–2954, 1990.

[20] C. Canali, G. Ottaviani, and A. Alberigi-Quaranta, “Drift velocity of electrons and holes and associated anisotropic effects in silicon,” *J. Phys. Chem. Solids*, vol. 32, pp. 1707–1720, 1971.

[21] P. M. Smith, M. Inoue, and J. Frey, “Electron velocity in Si and GaAs at very high electric fields,” *Appl. Phys. Lett.*, vol. 37, pp. 797–798, 1980.

[22] C. Jacoboni and P. Lugli, *The Monte Carlo Method for Semiconductor Device Simulation*. New York: Springer, 1989.

[23] G. Persky and D. J. Bartelink, “High-field diffusivity of electrons in silicon,” *J. Appl. Phys.*, vol. 42, pp. 4414–4421, 1971.

[24] C. Canali, C. Jacoboni, G. Ottaviani, and A. Alberigi-Quaranta, “High-field diffusion of electrons in silicon,” *Appl. Phys. Lett.*, vol. 27, pp. 278–280, 1975.

[25] ISE Integrated Syst. Eng. AG, “DIOS$_{ISE}$ Ref. Manual,”, 2002.

[26] ISE Integrated Syst. Eng. AG, “DESSIS$_{ISE}$ Ref. Manual,”, 2002.

[27] A. Wettstein, A. Schenk, and W. Fichtner, “Quantum device-simulation with the density-gradient model on unstructured grids,” *IEEE Trans. Electron Devices*, vol. 48, pp. 279–284, 2001.

[28] D. B. M. Klaassen, J. W. Slotboom, and H. C. de Graaff, “Unified apparent bandgap narrowing in n- and p-type silicon,” *Solid-State Electron.*, vol. 35, pp. 125–129, 1992.

[29] M. A. Darwish, J. L. Lentz, M. R. Pinto, P. M. Zeitzoff, T. J. Krutsick, and H. H. Vuong, “An improved electron and hole mobility model for general purpose device simulation,” *IEEE Trans. Electron Devices*, vol. 44, pp. 1529–1538, 1997.

[30] S. Keith, F. M. Bufler, and B. Meinerzhagen, “Full band Monte-Carlo device simulation of an 0.1 μm n-channel MOSFET in strained silicon material,” in *Proc. ESSDERC*, vol. 27, H. Grünbacher, Ed., Stuttgart, Germany, 1997, pp. 200–203, Editions Frontières.

[31] C. Jungemann, S. Keith, F. M. Bufler, and B. Meinerzhagen, “Effects of band structure and phonon models on hot electron transport in silicon,” *Elec. Eng.*, vol. 79, pp. 99–101, 1996.

[32] F. M. Bufler, P. Graf, S. Keith, and B. Meinerzhagen, “Full band Monte Carlo investigation of electron transport in strained Si grown on $Si_{1-x}Ge_x$ substrates,” *Appl. Phys. Lett.*, vol. 70, pp. 2144–2146, 1997.

[33] M. Lundstrom, “Scattering theory of the short channel MOSFET,” in *IEDM Tech. Dig.*, 1996, pp. 387–390.

[34] F. Assad, Z. Ren, S. Datta, M. Lundstrom, and P. Bendix, “Performance limits of silicon MOSFET’s,” in *IEDM Tech. Dig.*, 1999, pp. 547–550.

[35] M. S. Lundstrom, “On the mobility versus drain current relation for a nanoscale MOSFET,” *IEEE Electron Device Lett.*, vol. 22, pp. 293–295, 2001.

[36] M. Lundstrom and Z. Ren, “Essential physics of carrier transport in nanoscale MOSFETs,” *IEEE Trans. Electron Devices*, vol. 49, pp. 133–141, 2002.

F. M. Bufler received the Dipl.Phys. degree from the RWTH Aachen, Aachen, Germany, in 1992 and the Ph.D. degree from the Universität Bremen, Bremen, Germany, in 1997.

In 1992, he joined the Institut für Theoretische Elektrotechnik, RWTH Aachen, Aachen, Germany, and moved in 1995 together with the group of Prof. B. Meinerzhagen to the Institut für Theoretische Elektrotechnik und Mikroelektronik, Universität Bremen, Germany. Since 1997, he has been with the Institut für Integrierte Systeme, ETH Zürich, Switzerland, working in the field of TCAD on Monte Carlo device modeling and transport theory.

Yoshinori Asahi (M'88) was born in Kyoto, Japan. He received the B.S., M.S., and Ph.D. degrees in chemistry from Kyoto University, Kyoto, Japan.

He joined Toshiba Corporation in 1981 where he has been engaged in the development of CMOS technology for Logic LSI. From 1988 to 1989, he was a Visiting Scholar at Stanford University, Stanford, CA, where he studied process and device modeling. His current interests are technology CAD and its application to device development.

Dr. Asahi is a member of the IEEE Electron Devices Society and the Institute of Electronics, Information, and Communication Engineers of Japan.

Hisao Yoshimura (M'99) received the B.S., M.S., and Ph.D. degrees in electronic engineering from the University of Tokyo, Japan, in 1985, 1987, and 1990, respectively. His Ph.D. work involved the optical properties of quantum-well heterostructures based on III–V semiconductors.

In 1990, he joined the Semiconductor Device Engineering Laboratory, Toshiba Corporation, where he was engaged in the development of CMOS technology for SRAM and Logic LSI. From 1993 ot 1994, he was a member of the IBM/Siemens/Toshiba 0.25-μm DRAM project at the IBM Advanced Semiconductor Technology Center (ASTC), Hopewell Junction, NY. Since 1994, he has been engaged in the research and development of CMOS Technology from 0.15-μm to 50-nm scales. He is currently with Advanced Logic Technology Department, Toshiba Corporation, Semiconductor Company, Yokohama, Japan. His current work includes CMOS device development at sub-50-nm dimensions and scaling considerations of CMOS devices into the sub-10-nm length.

Dr. Yoshimura is a member of the IEEE Electron Devices Society and the Japan Society of Applied Physics.

Christoph Zechner was born in Graz, Austria, in 1972. He received a Dipl.-Ing. degree from the Technical University of Graz, Graz, Austria, in 1996 and the Ph.D. degree from the University of Konstanz in 2000 for experimental work and computer simulations of silicon solar cells.

In 2000, he joined ISE AG, Zurich, Switzerland. His main interest is the calibration of implantation and diffusion process simulation and the computer simulation of MOSFETs.

A. Schenk was born in Berlin, Germany, in 1957. He received the Diploma in physics and the Ph.D. degree in theoretical physics from the Humboldt University Berlin (HUB), Berlin, Germany, in 1981 and 1987, respectively.

In 1987 he became a Research Assistant with the Department of Semiconductor Theory, HUB, and in 1988 he joined the R&D division of WF Berlin. From 1987 until 1991, he was working on various aspects of the physics and simulation of optoelectronic devices, especially infrared detector arrays, and the development and implementation of physical models for modeling infrared sensors. He is now with ETH, Zurich, Switzerland, as a Senior Lecturer at the Integrated Systems Laboratory. His main activities are in the development of physics-based models for simulation of submicron silicon devices.

Dr. Schenk is a member of the German Physical Society (DPG).

Wolfgang Fichtner (M'79–SM'84–F'90) received the Dipl.Ing. degree in physics and the Ph.D. degree in electrical engineering from the Technical University of Vienna, Vienna, Austria, in 1974 and 1978, respectively.

From 1975 to 1978, he was an Assistant Professor in the Department of Electrical Engineering, Technical University of Vienna. From 1979 through 1985, he worked at AT&T Bell Laboratories, Murray Hill, NJ. Since 1985, he has been a Professor and Head of the Integrated Systems Laboratory at the Swiss Federal Institute of Technology (ETH), Zurich. In 1993, he founded ISE Integrated Systems Engineering AG, a company in the field of technology CAD.

Dr. Fichtner is a member of the Swiss National Academy of Engineering and a corresponding member of the Austrian Academy of Sciences. In 2000, he received the IEEE Grove Award.